



Using the Corner Reflection for Depth Evaluation of Surface Breaking Cracks in Concrete by Ultrasound

Ute Rabe¹ · Sergey Pudovikov¹ · Hans-Georg Herrmann¹ · Herbert Wiggerhauser² · Prathik Prabhakara³ · Ernst Niederleithinger³

Received: 20 September 2022 / Accepted: 25 April 2023
© The Author(s) 2023

Abstract

The corner echo is a well-known effect in ultrasonic testing, which allows detection of surface breaking cracks with predominantly perpendicular orientation to the surface as, for example, corrosion cracks in metal pipes or shafts. This echo is formed by two planes, the surface of the crack and the surface which the crack breaks. It can also be classified as a half-skip method, since a reflection of the pulse occurs on the backwall before the reflection at the defect takes place. In combination with the diffraction from the crack tip, the corner echo also allows crack sizing. As shown in this paper, the corner reflection can be used in civil engineering for nondestructive inspection of concrete. Commercially available low frequency ultrasonic arrays with dry point contact sources generate SH transversal waves with sufficient divergence of the sound field in order to detect corner reflections. Ultrasonic line-scans and area-scans were acquired with a linear array on flat concrete specimens, and the data were reconstructed by the Synthetic aperture focusing technique. If the angles and the area of reconstruction are chosen accordingly, the corner echo reflection can be distinguished from other ultrasonic information. The corner echo can thus be used as a method for deciding whether a crack is a partial-depth crack or a full-depth crack and thus for obtaining a statement about crack depth. This paper presents corresponding experimental results obtained on concrete specimens with artificial test defects and cracks induced under controlled conditions.

Keywords Ultrasonic testing of concrete · corner echo · surface breaking cracks · nondestructive testing in civil engineering · synthetic aperture focusing technique

1 Introduction

Cracks are a natural constituent of concrete, ranging from microcracks to sizes and widths, which are clearly visible to the human eye. They are caused by shrinkage, static or dynamic mechanical loads, chemical processes or temperature changes during hardening and operational life. Their appearance at the surface may tell the experienced inspector the cause for the cracks to develop. Cracks due to shrinkage have a network like structure and may not reach deep into the concrete component, while cracks which follow load

directions or prestressing tendons may be an indication of overloading. While surface opening cracks can be identified through visual inspection, their subsurface shape and dimension may be unknown. Cracks with small surface openings (< 0.1 mm) can be tolerated [1], whereas larger cracks may affect the durability of the structure by allowing fast transport of gaseous and liquid substances and thus revoke the natural corrosion protection of steel reinforcement. A comprehensive overview of cracks in concrete is compiled in [2].

The dimension of the cracks is especially of interest in concrete structures which function as a barrier against environmental hazards, where cracks can destroy the barrier function. Such barriers are in widespread use in industry and public structures and may have a variety of designs. The crack geometry must be examined in situations where the structure is only accessible from one side and where proof is required that the crack is not fully penetrating the concrete slab. Naturally, nondestructive methods are preferred

✉ Ute Rabe
ute.rabe@izfp.fraunhofer.de

¹ Fraunhofer Institute for Nondestructive Testing IZFP, Campus E3.1, Saarbrücken, Germany

² Berlin, Germany

³ Bundesanstalt für Materialforschung und -prüfung (BAM), Unter den Eichen 87, Berlin, Germany

techniques to execute such a test. In summary, there are several reasons to provide a nondestructive technique which can decide whether a surface breaking crack is a partial-depth crack or a full-depth crack. The inspection with ultrasound will require equipment able to cope with the dimensions of the barrier component and test requirements. A multilayer design of a slab barrier will not allow testing beyond the first layer of acoustic isolation.

Ultrasonic techniques, especially with the application of transducer arrays and subsequent known acoustic methods for crack detection and crack depth measurement in concrete are impact echo and ultrasound pulse-echo. A British standard [3] describes two ultrasonic methods for crack depth measurement in concrete based on time-of-flight diffraction (TOFD) measurement. Similar time-of-flight techniques are known for crack depth measurement with impact-generated stress waves [4]. TOFD evaluates the first arrival of the pressure wave, which is transmitted and diffracted by the crack tip. However, though methods which rely on crack tip diffraction and first arrival detection work well with artificial defects like notches or saw cuts, their results are often much more difficult to interpret in case of real cracks, as observed by several research groups, see e.g. [5]. It is also possible to use surface wave transmission for crack depth estimation [6, 7]. Surface waves can be excited by impacts, either using a hammer blow or an automatic solenoid impactor, see e.g. [8]. The force normal to the surface, which results from the impact, can be modelled as a point source, which radiates more than half of its energy as a Rayleigh wave [9]. This makes surface wave application with impact-echo method very efficient. In practical application, the theoretical spectral dependence of energy transmission is superimposed by near-field scattering of the crack tip, variations in coupling condition of the emitters and receivers on rough concrete surfaces, and interfering influences from steel reinforcement, other heterogeneity and noise sources. As compensation, a self-calibration procedure was developed [6, 7]. Application of air-coupled sensors [10] or air-coupled ultrasonic transducers [11] is reported to improve the results. A relatively new approach is based on using the diffusion of incoherent ultrasonic energy to estimate crack depth [12–14]. However, partially closed cracks, allowing some part of the ultrasonic energy to transmit, are difficult to characterise with this method [14] and in our opinion also affect most of the other methods described above.

Ultrasonic transducers, especially dry point contact transducers (DPC) [15, 16], allow the excitation of bulk shear waves with well-defined polarisation and centre frequency. Area scans with transmitting-receiving transducers or with linear arrays generate more ultrasonic information than single point measurements. Furthermore, post-processing of ultrasonic line- or area-scan data with the synthetic aperture focusing technique (SAFT) provides tomographic cross-sections of the examined component and improves the

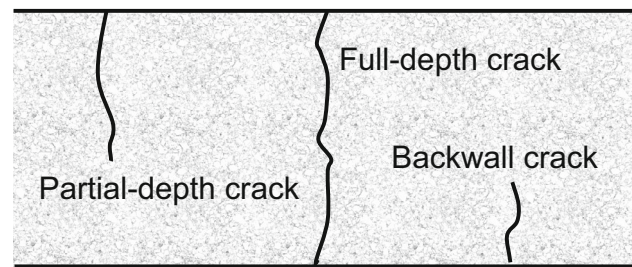


Fig. 1 Definition of vertical crack types in concrete

signal-to-noise ratio of the indications in case of heterogeneous materials, which scatter the ultrasonic waves [15]. Commercially available arrays allow the practical on-site application of the shear-wave tomography. Several successful applications of the technique are reported. For example, component backwalls, reinforcement bars and horizontal delaminations were successfully imaged with shear wave arrays [17]. In conventional ultrasonic testing of metals with longitudinal wave arrays, the full matrix capture (FMC) measurement procedure with total focusing method (TFM) reconstruction has been shown to be very suitable for crack depth determination [18]. An early successful application of 3D-SAFT to image the faces of a real crack in concrete is reported in [19]. In this study, an array of broad band ultrasonic longitudinal wave transducers (50–250 kHz) was placed at one side of the crack for ultrasound transmission. At the other side of the crack the ultrasonic signal was detected with an optical vibrometer, which was scanned with a step size of 5 mm. Data of several sending positions and corresponding receiver scans were processed with 3D SAFT and superimposed. However, using conventional contact probes that rely on coupling agents in combination with an optical vibrometer is much more complicated for field measurements than a scan with a DPC array. Although the depth of notches was successfully imaged with DPC shear wave arrays, depth measurement of real cracks was not successful so far [20].

To approach the difficult task of crack dimension measurement in concrete, this paper answers a simple question: “Is the crack a partial-depth crack or a full-depth crack?” (Fig. 1). The method we present in the following can be used either to check whether a crack is a full-depth crack or not, or it can be used to find vertical cracks that are open to the backwall of flat concrete components, which are only accessible from one side. The measurement and evaluation procedure will be first demonstrated using concrete blocks with 250 mm thickness with cracks created under controlled condition. Application to thicker components will be discussed in the following chapters.

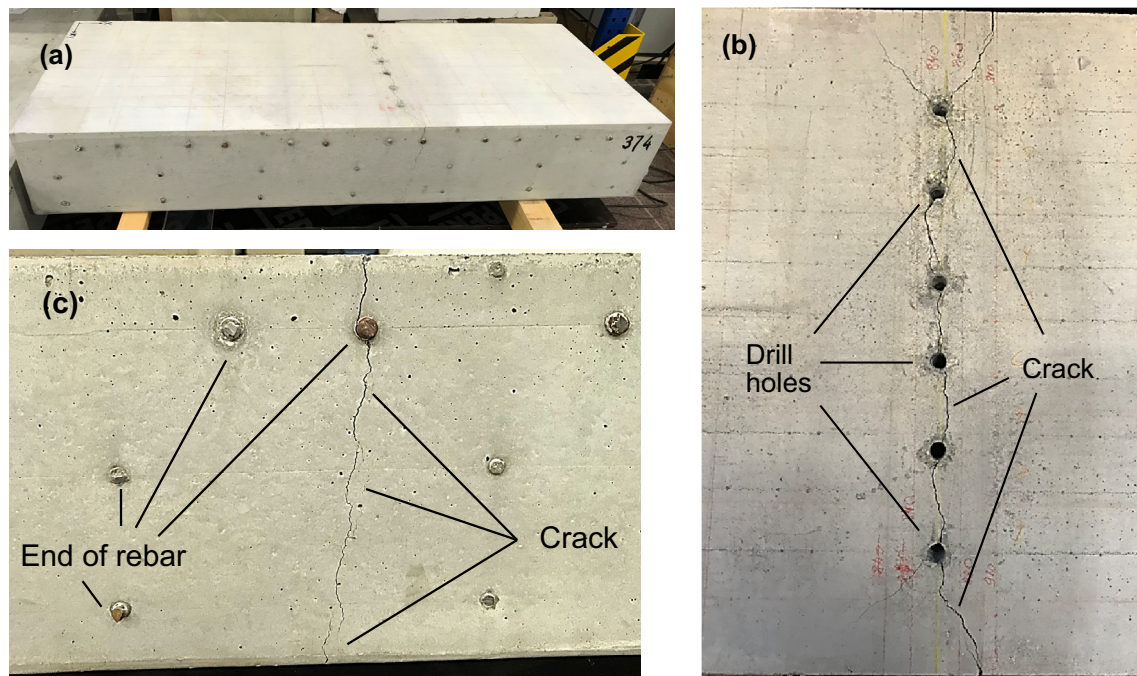


Fig. 2 Photo of concrete block #6 featuring the full-depth crack: **a** photo of the entire specimen, **b** and **c** enlarged image of the crack area (**b** on the top surface, here drill holes used for crack initiation are visible, **c** on the side face)

2 Concrete Specimens with Reference Defects

Concrete blocks with notches and cracks initiated under controlled conditions [21] were utilised for the method development. In ultrasonic testing, it is common to use saw cuts or notches as reference defects representing cracks. Such artificial defects are helpful for basic investigations. However, methods that are successful in finding and determining the depth of saw cuts may not necessarily work with real cracks. A saw cut has a constant width over its full depth; it therefore represents a complete separation down to its tip. The opening of real cracks, however, varies over their length and depth. The crack faces can touch, which leads to contact points and possible transfer of acoustic energy. Steel reinforcement bars, which may bridge the crack, are present in most cases. Concrete is a heterogeneous material consisting of aggregates, air filled pores, and cement matrix. The crack faces do not always end in one well-defined line, but rather, a damaged zone with a multitude of small cracks or pores is possible instead of a well-defined crack tip. Furthermore, the faces of a real crack are not perfect planes, but rough surfaces with variable orientation.

For the research reported here, six concrete blocks of equal size were used. A photo of one of the blocks is shown in Fig. 2. In an empirical study, a method was developed to create cracks with controlled depth [21]. Concrete blocks with the dimensions 1500 mm × 600 mm × 250 mm (length × width × thickness) were designed with concrete quality

C30/37 and a maximum aggregate size of 16 mm. All blocks contain three layers of reinforcement, each layer consisting of steel bars with 8 or 12 mm diameter oriented parallel to the block's top and bottom faces. The reinforcement layout is designed to limit the crack development, stabilise the crack, and to guide the crack growth. The highest and lowest layers placed in a depth of 40 mm relative to the top and bottom surfaces are identical for all blocks. The depth of the centre layer varies to limit the intended crack depth. It is positioned either 85, 125, or 165 mm deep relative to the surface. The coordinate system used for the measurements and the general orientation of the crack or notch is explained in Fig. 3. The photo of the side face included in Fig. 2 shows the full-depth crack and the ends of the rebars in width direction in the respective block. In the case presented in the image, the middle layer was at position $z = 125$ mm. Table 1 lists the properties of all specimens. Here and in the following, an index extension is added to each ID to illustrate the kind of defects which the specimen includes: “-pdc” for the “partial-depth crack”, “-fdc” for the “full-depth crack”, “-notch” for notch and “-free” if no defects inside are supposed.

Specimen #4-free is free of artificial defects and serves as a reference; specimen #5-notch features a notch with a depth of 72.5 ± 2.5 mm, which was created without cutting the rebars. The width of the notch is 0.9 ± 0.1 mm. The specimens #1-pdc, #2-pdc and #3-pdc have partial-depth cracks. To generate these cracks, a row of six holes (see Fig. 2) were filled with expansion mortar [21]. The expansion of the mortar due to curing creates mechanical stress in the block

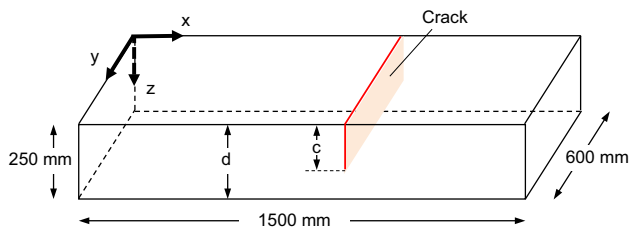


Fig. 3 Schematic sketch of a concrete specimen, thickness d , with defect, depth c . The zero point of the coordinate system is set to the upper left corner of the specimen

volume around the holes. A crack forms, which splits the surface between the holes. If the diameter and depth of the holes are within a certain limit, the crack propagation stops at depth values around the middle layer of the reinforcement. The width of these cracks on the top surface ranges between 0.05 and 0.25 mm. Further details regarding the controlled crack production procedure are described in [21]. In specimen #6, the crack was created in two steps. First, the drill holes were filled with expansion mortar and a partial-depth crack was initiated. In a second step, the width and the depth of the holes was increased, and the holes were filled with expansion mortar again until a full-depth crack formed. The specimen was rotated once to inspect the back surface and to verify the full penetration of the crack to the opposite side. The average width of the full-depth crack on the top surface is 0.6 mm. In contrast to the other specimens in Table 1, which were examined with ultrasound after the cracks had been generated, specimen #6 was imaged in different conditions: Before crack generation, with partial-depth crack and with full-depth crack.

3 Description of the Test Equipment and the Measurement Procedure

Low frequency DPC transducers [15, 16] as transmitters and receivers allow an efficient transmission and reception of ultrasonic signals in concrete. For the work reported here,

a commercially available acoustic shear wave device, A1040 MIRA (ACS Group, Moscow, Russia), was used. The A1040 MIRA is a linear array with $N = 12$ elements, the line-pitch in the active aperture is $p = 30$ mm (see Fig. 4c). The distance between the first element and the last element is 330 mm, and the offset between the centre of the instrument (nominal instrument position) to the first element is 165 mm.

Each linear element is formed by a row of four directly coupled DPC with a spacing of 25 mm within the passive aperture. This specific combination of transducers is used to increase the signal amplitudes when transmitting and receiving and to suppress surface wave emission in the y -direction. The direction of vibration of the shear DPC and hence the direction of vibration of the transmitted shear waves is in the y -direction, perpendicular to the x - z plane. The source can be seen as a point contact as the tip radius is in the mm range and therefore one order of magnitude smaller than the ultrasonic wavelength λ (typical values are: shear wave velocity $V = 2700$ m/s, frequency $f = 50$ kHz, $\lambda = 54$ mm). The theoretical angular directivity of such an array of shear horizontal (SH) point sources is independent of the angle in the x - z plane [22–24].

One measurement with the MIRA consists in the acquisition of 66 time signals. If element n acts as a transmitter, the time signals received by elements $\{n + 1, n + 2, \dots, N\}$ are stored. After 11 transmitting events, the measurement is complete with its sum of 66 transmitter-receiver combinations and 66 corresponding A-scans. Figure 4c illustrates the beam path of the 66 transmitter-receiver combinations in case of a plane parallel reflector at 250 mm depth d (backwall). Independent of the amount of the distance d , the ultrasonic “rays” hit the backwall at 21 equidistant points with a pitch of $p/2 = 15$ mm. Note, that this is an idealised model, which assumes a perfectly flat reflector parallel to the surface. In dependence of the roughness, scattering and misalignment of the backwall, the actual ultrasonic energy transmission may deviate more or less from the ideal condition.

Either line scans (Fig. 5a) or area scans consisting of several lines (Fig. 5b) were manually taken with the MIRA

Table 1 Properties of the concrete specimens

Block ID	Defect type	Centre rebars z -coordinate (mm)	Defect depth c at side faces (mm)	x -position of defect (mm)
1-pdc	Crack	85	91 ± 45	855 ± 11
2-pdc	Crack	125	98 ± 10	861 ± 10
3-pdc	Crack	165	135 ± 11	865 ± 8
4-free	Defect free reference	125	—	—
5-notch	Notch	125	72.5 ± 2.5	748 ± 3
6-fdc	Full-depth crack	125	250	860 ± 15

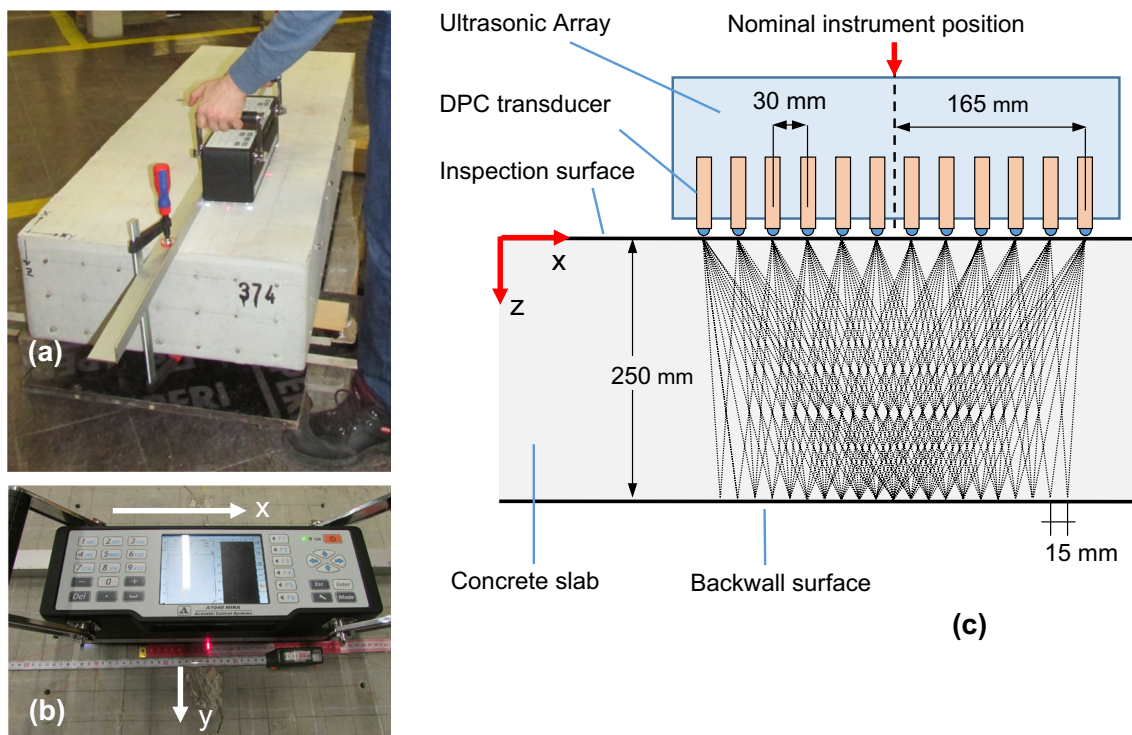


Fig. 4 **a, b** Images of the A1040 MIRA taken during the measurements. **c** Schematic sketch of the 12 elements of the MIRA array and 66 lines representing the shortest distance between all transmitters and receivers in case of specular reflection from a plane backwall

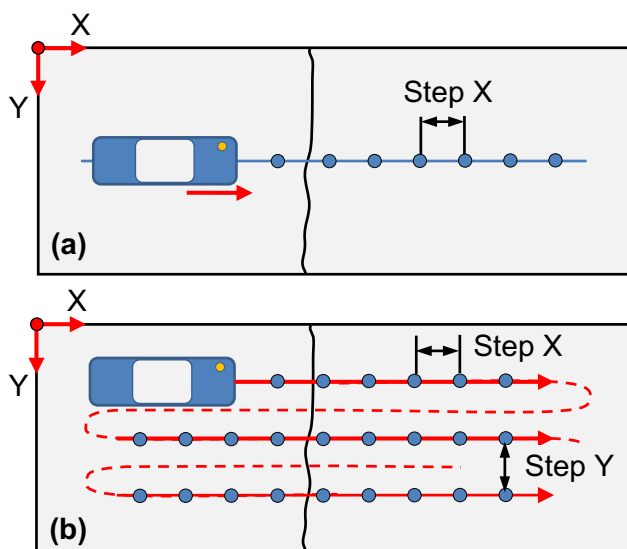


Fig. 5 Image acquisition and scanning procedure with the linear array A1040 MIRA: **a** line scan perpendicular to the crack, **b** area scan as a set of line scans

instrument. The length axis of the instrument was aligned in x -direction, which was also the direction of the line scans. The step size was 30, 60 or 90 mm in x -direction (line direction). The spacing between the lines in y -direction was 50 mm in case of the area scans. Simple mechanical aids such

as rulers or grids drawn on the surface were used for instrument alignment. The length of the electrical excitation pulses was either 1 or 1.5 cycles. The nominal centre frequency was set to 50 kHz. The analog gain was adjusted individually depending on the ultrasonic attenuation and thickness of the specimen. All measurements were saved in *map mode*, a program feature of the MIRA instrument, which allows to save A-scan arrays. The raw data were read from the instruments and transferred to the servers of IZFP for further evaluation.

4 SAFT Reconstruction

The SAFT reconstruction is a back-projection of the acquired acoustic data into the discretized model of the investigated component volume [15, 25, 26]. SAFT is based on several assumptions. Among others it is assumed that each pixel/voxel of the object model is a point reflector which is a source of secondary waves. Furthermore, a 180° divergence of the sound field of each element in the ultrasonic array is assumed. Therefore, the wave emitted by each ultrasonic array element reaches all volume points and the element can receive the ultrasonic responses from all points if it acts as a receiver.

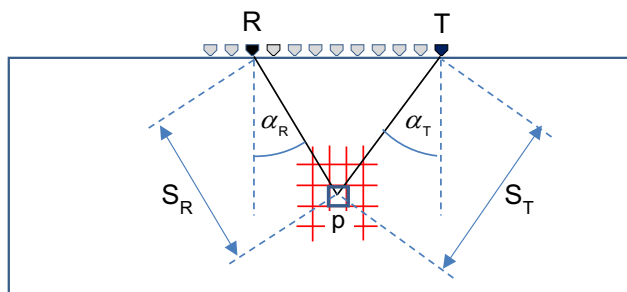


Fig. 6 Principle of 2D SAFT reconstruction

Figure 6 shows schematically the back-projection in case of 2D SAFT. The value I_p of the pixel p in the reconstruction plane is the sum of the corresponding amplitude values $A^{TR}(t)$ from all acquired A-scans (Eq. 1). Here, T is the transmitter, R is the receiver, A^{TR} is the time signal of the combination TR , t is the time of flight from transmitter T to the receiver R through the pixel p , S_R and S_T are the distances from array elements to the pixel, and V is the sound velocity. Optionally, an angle-weighting with the cosine function can be applied to minimise the influence of the surface waves in the SAFT reconstruction images. In this case each value $A^{TR}(t)$ is multiplied by $K = \cos(\alpha_T)\cos(\alpha_R)$ before the summation. The direction-dependent apodization coefficient K is not related to the directional characteristic of the DPC, since the sound field of the SH wave in the inspection plane is non-directional and uniform for all the directions. This apodization is used to artificially reduce the influence of the surface wave, which propagates between the array sensors. Unless explicitly mentioned (as in Figs. 12 and 13), in this work, surface wave suppression was always applied in the standard full-angle SAFT reconstruction to make the near-surface volume indications as for example indications from the upmost reinforcement layer more clearly visible.

$$I_p = \sum_{T=1}^{11} \sum_{R=T+1}^{12} A^{TR}(t = \frac{S_T + S_R}{V}) \quad (1)$$

As an example, Fig. 7 illustrates the reconstruction of a single-point MIRA measurement taken on the concrete block #4-free (Fig. 7a). After projection of only one A-scan from transmitter 1 and receiver 2 (Fig. 7b), the assumed 180° directivity and the applied cosine-weighting are visible. Each additional projected ultrasonic signal creates a more precise result. A *synthetic aperture* is formed and the projected signals interfere constructively in the locations of reflectors and destructively in absence of reflectors. As a rule, a larger aperture increases the information in the reconstructed image. In Fig. 7c 11 signals (transmitter 1, receivers 2–12) are projected, and in Fig. 7d the contributions of all 66 signals were added. The reconstructed image (*B-scan*) now shows the locations of the rebars and the backwall, which were in

the cross-section area illuminated by the respective MIRA measurement.

If the data from several positions of the ultrasonic array are acquired, a *compound-B-scan* can be calculated by processing all data. The compound-B-scan in Fig. 8 is a 2D SAFT image calculated from a line-scan consisting of 13 equidistant positions of the MIRA array, step width 90 mm.

Figure 9 shows examples of compound-B-scans calculated by 2D SAFT from area scans taken on the concrete specimens listed in Table 1. The images were obtained with IZFP software, which was written in MATLAB [27]. The reconstruction of a single line at $y = 300$ mm is shown as a representative example. The backwall at a depth of 250 mm is well visible in all cases as a red horizontal line-shaped indication. Some of the rebars are visible as dot-like indications. The reconstruction area was extended to a depth $z = 600$ mm. This means that the mirror plane is included; the horizontal indication at 500 mm depth is an ultrasonic image of the sample top surface. In Fig. 10, which repeats Fig. 9h, all mentioned indications are labeled, to make the interpretation of the images in Fig. 9a–h easier.

As can be seen in Table 1, all specimens, except the reference #4-free (Fig. 9d) and the specimen #6-free (Fig. 9f) in defect-free state, feature a notch or a crack at an x -position between 748 and 865 mm. A corresponding disruption or disturbance of the backwall indication is well visible in all compound-B-scans. There are also indications at small z -values close to the surface at the defect position and in some cases more indications at different depth values. Another observation worth noting with respect to specimen #4-free (Fig. 9d): Here, the backwall indication is not a straight line as would be expected in the defect-free case, but some interruptions are visible. In summary, it can be concluded after evaluating the 2D-SAFT images obtained by standard processing: Although the x -position of the defect can be easily identified in all cases, it is not possible to clearly determine the depth of the crack or notch.

5 Corner Echo Visualisation Using Linear DPC Transducer Arrays

A corner reflector is formed by two planes, which are perpendicular to each other as shown schematically in Fig. 11. The white area in Fig. 11 is the acoustic plane, the grey areas are mirror planes. The green lines show the sound path for the corner reflection between a transmitter T and a receiver R on the specimen surface. The ultrasonic wave reflects once at the backwall (point 2) and once at the vertical wall (point 1). According to the principles of geometric acoustics, the sound path from transmitter T to receiver R with two reflections on the vertical and horizontal surfaces is equivalent to the direct path between the transmitter T and an imaginary

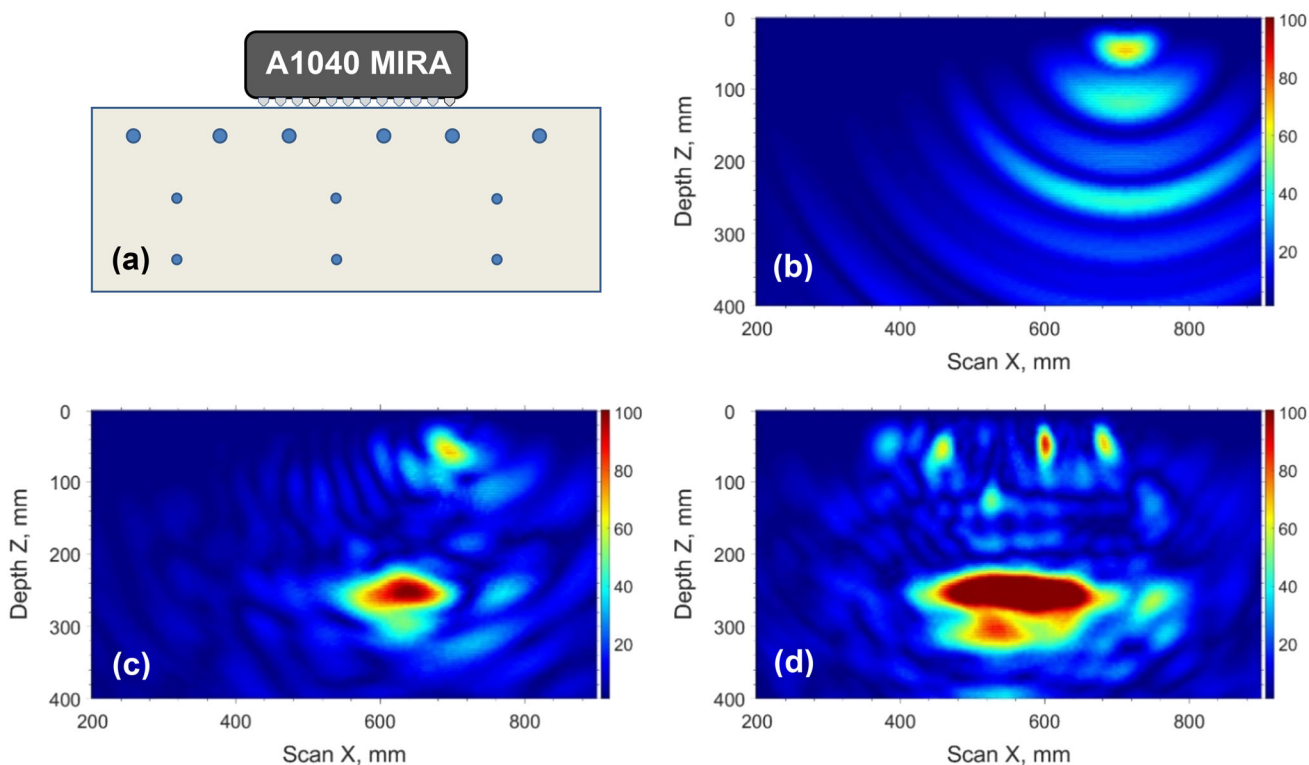


Fig. 7 a schematic sketch of the ultrasonic array in the measurement position, b–c 2D SAFT reconstruction of the ultrasonic data of a single-point measurement taken on the concrete specimen #4-free: b one A-scan, c 11 A-scans, d 66 A-scans

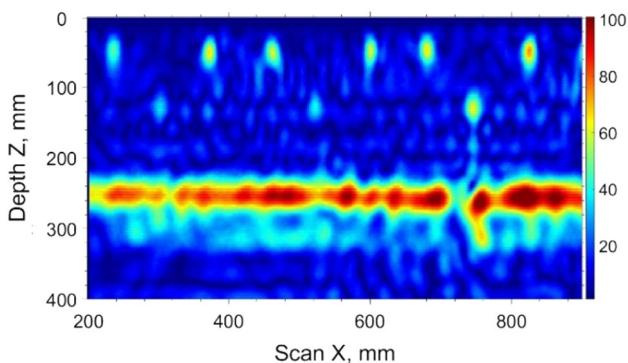


Fig. 8 Compound-B-scan of specimen #4-free calculated from a line scan taken with the MIRA, 13 instrument positions, start position at $x = 200$ mm, step width $\Delta x = 90$ mm

receiver R' . Here R' is symmetrical to the point R^* (the horizontal plane is the symmetry axis), and R^* is symmetrical to R in the vertical plane (Fig. 11).

After simple geometrical derivations, we can localize the points 1 and 2. Since the lateral position of point 2 is exactly in the middle between T and R^* , we can find Δx :

$$\Delta x = r + a - 0.5(2r + a) = 0.5a \tag{2}$$

and after that Δz . For this, we evaluate tangent of α :

$$\tan \alpha = \frac{a + r - \Delta x}{d} = \frac{r + 0.5 \cdot a}{d}, \Delta z = \Delta x \tan \alpha = \frac{0.5 \cdot a \cdot d}{r + 0.5 \cdot a} \tag{3}$$

where r is the distance between the receiver and the vertical wall, a is the distance between transmitter and receiver, and d is the object thickness. Such a corner is known as a retroreflector because each wave arriving under an angle α is reflected back under the same angle. The time-of-flight of the ultrasonic wave reflected by the corner depends only on the angle α and not on the distance between transmitter and receiver.

The effect of the reflection from a corner reflector is widely used in the ultrasonic inspection of weld joints to detect vertical cracks in the weld root or for the detection of fatigue cracks in shafts or tubes. Commonly, single pulse-echo transducers or phased arrays are used, which generate and receive vertically polarised shear waves (SV) under an angle of 45° in the component under inspection. The intensity of the reflection of SV waves from the corner is angle-dependent due the mode conversion, which occurs by the sound reflection on the steel-air surface [28]. The reflection coefficient of the SV wave for steel/air is almost 1 for the angles $\alpha = 33^\circ$ – 57° and decreases sharply for angles $< 33^\circ$ and $> 57^\circ$ [28]. The usage of DPC transducer arrays like the MIRA makes

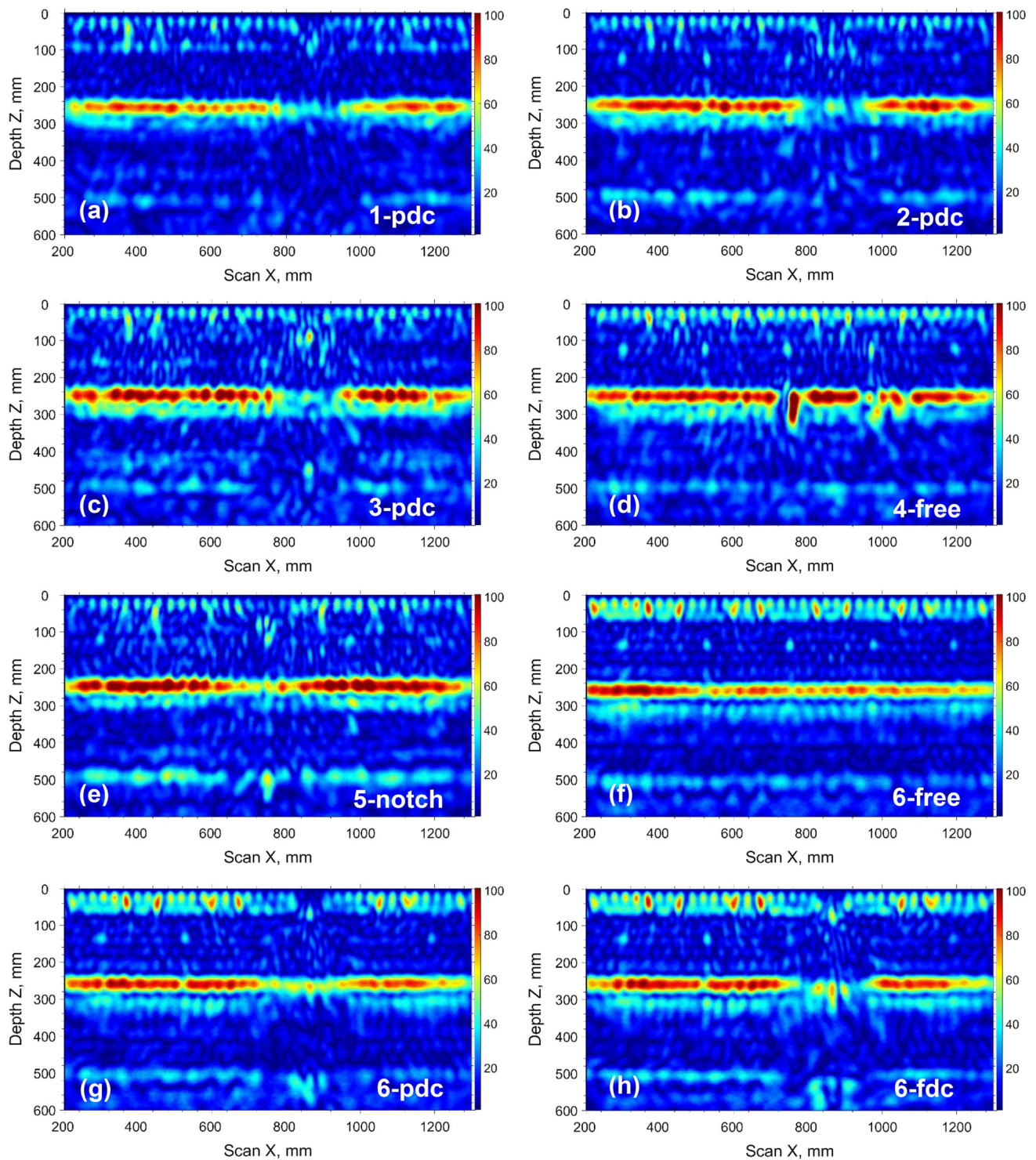


Fig. 9 Compound-B-scans of the specimens listed in Table 1 calculated from line scans at position $y = 300$ mm, start position $x = 200$ mm, step width $\Delta x = 90$ mm. **a–e** Specimen #1–#5. Note that specimen

#6 was scanned in three different conditions: **f** without defect, **g** with partial-depth crack and **h** with full-depth crack

Fig. 10 Indications in the compound-B-scan of specimen #6 with full-depth crack

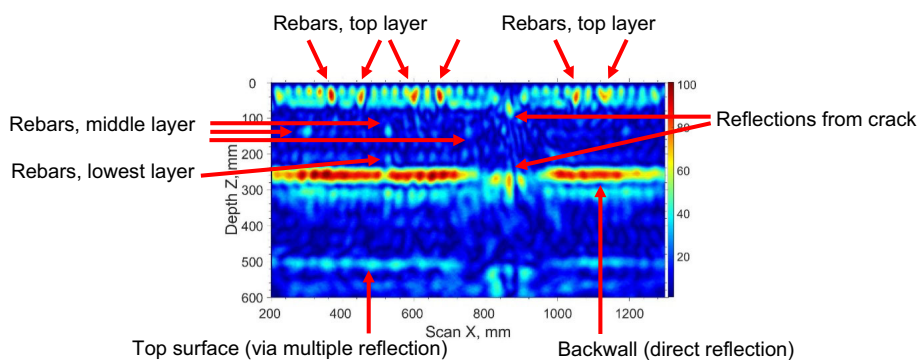
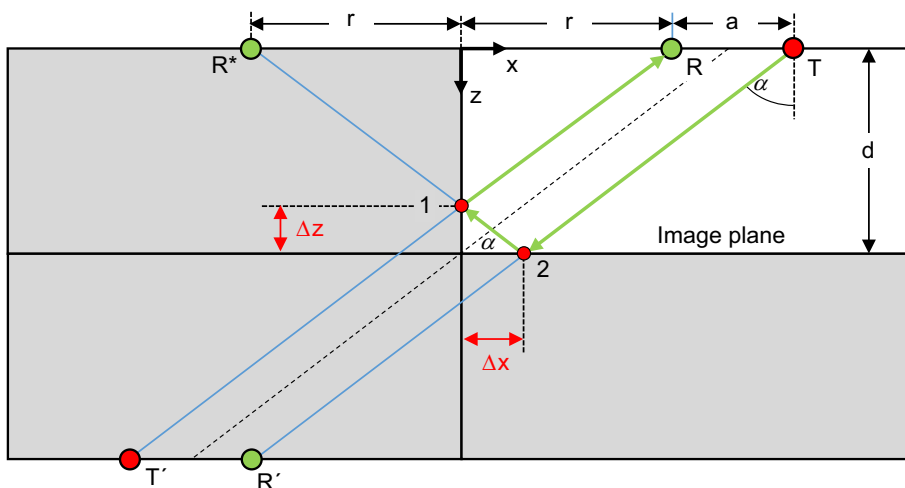


Fig. 11 Geometry of the corner reflector. The green arrows show the sound path between transmitter (T) and receiver (R) in case of specular reflection at a concrete-air interface. The white area is the acoustic plane. The grey areas are mirror planes



two important differences in comparison to the wide-spread inspection of metallic components. Firstly, the DPC transducers of the MIRA array generate horizontally polarised shear waves (SH). If the planes of the corner reflector are located in the plane perpendicular to the polarisation plane of the SH waves, no mode conversion on the object boundaries occurs, and the reflection coefficient is almost 1 for concrete/air for the whole range of angles α . Secondly, the DPC transducers are directly placed onto the surface without any wedged delay-line, which is commonly used in the UT inspection of metals to redirect the main lobe of the sound field into the desired direction. While for detection of vertical cracks in metals the acoustical energy is concentrated under 35° – 55° to meet the optimal reflection angle, a DPC transducer generates a non-directional sound field [22–24]. Alternative methods to visualise the corner indication are therefore necessary.

The standard SAFT reconstruction as provided in Fig. 9 shows the area below the MIRA instrument. In order to receive a corner echo, however, the sensors must be displaced in x -direction relative to the corner so that the corner can be insonified at an oblique angle of incidence. The MIRA array consists of 12 elements with a pitch of 30 mm and a maximal

distance of 330 mm. Figure 12a–d show the schematic acoustic path of the corner reflection for all transmitter-receiver combinations of the MIRA. The distance between the nominal position of the MIRA instrument and the corner was varied as well as the component thickness. The corner is located at $x = 0$. In case of an ideal 90° corner, the backwall is always hit at 11 equidistant points (pitch 15 mm) with a maximum distance of $\Delta x = 330 \text{ mm}/2 = 165 \text{ mm}$ to the corner. This is independent of the component thickness and instrument x -position relative to the corner. The distribution of the reflection points on the vertical corner wing depends on the specimen thickness and on the instrument position. According to Eq. (3), the highest point of reflection is located at

$$\Delta z = \frac{0.5 \cdot 330 \text{ mm} \cdot d}{x_{Mira} - 165 \text{ mm} + 0.5 \cdot 330 \text{ mm}} = \frac{d \cdot 165 \text{ mm}}{x_{Mira}} \quad (4)$$

This leads to the conclusion that a distance of the nominal position of the MIRA array of approximately $x_{MIRA} = d$ is a good choice, because in this case $\Delta z = \Delta x$, i.e., the acoustic energy is well concentrated in the corner. With increasing distance of the instrument to the corner, the ultrasonic distance increases, which leads to less received ultrasonic energy due to beam divergence, scattering and absorption.

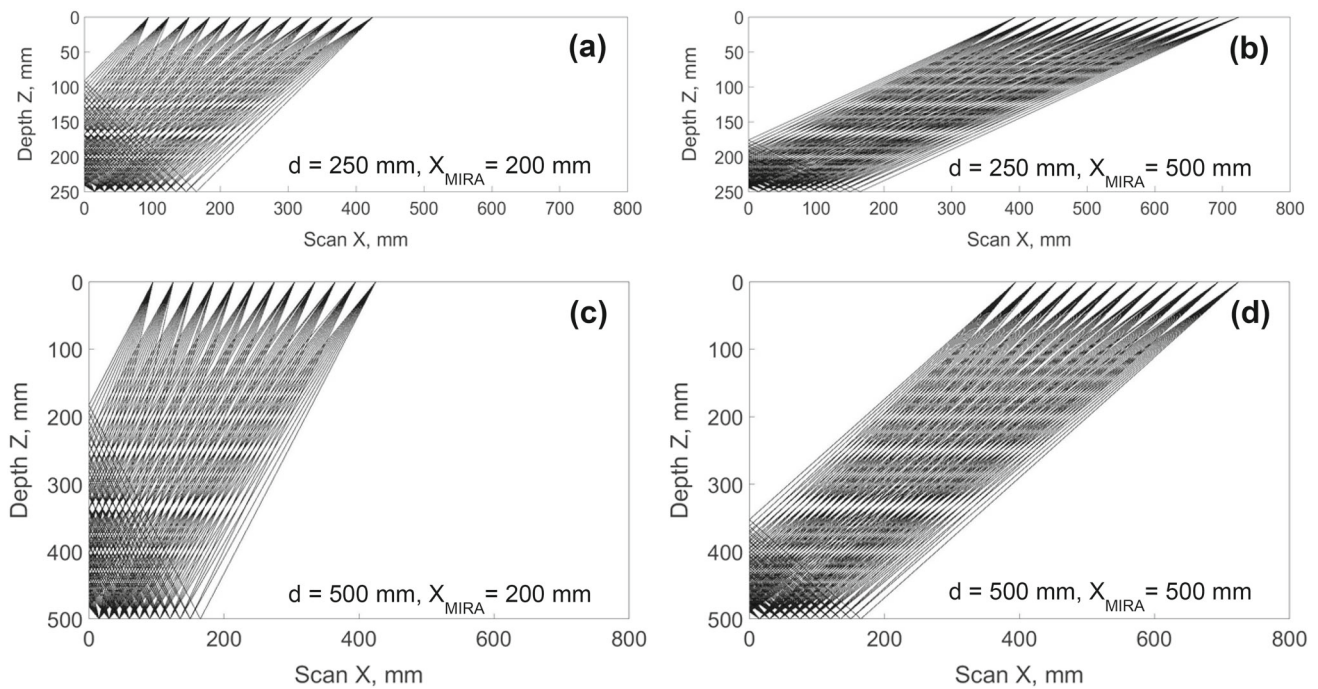


Fig. 12 Distribution of reflective points on the corner surfaces and sound path for all 66 MIRA transmitter-receiver combinations for two component thicknesses and two MIRA positions relative to the corner

The backwall surface causes a strong reflection. If the thickness and the acoustic attenuation of the inspection object allow, more than one reflection of the ultrasonic pulse at the backwall will be detected. After the SAFT reconstruction, these reflections are presented in the image as equidistant lines at depth values which are multiples of the thickness d . As an example, Fig. 13a shows the reconstructed image of one measurement position on the specimen #6-free before the crack was produced. This position was chosen in the middle of the specimen's surface. The cosine-filtering was not applied. As a consequence, there are high intensity indications at the depth values 0–60 mm, which are caused by the surface waves between the transmitters and receivers. The backwall indication (1) is at depth $z = 250$ mm and the surface indication (2) at $z = 500$ mm. Signal (2) has lower intensity than the signal (1) due to attenuation of the acoustic waves. The schematic representation in Fig. 13b illustrates how the signals (1) and (2) are formed. Note that signal (2) is formed by a further reflection of the pulse at the component top and bottom surfaces.

Before considering full-depth cracks, the outer edges of the specimens can be examined as reference corners. As the side walls of the specimens are flat and exactly vertical, they are “ideal” corner reflectors. Figure 14a shows the reconstructed image of one measurement position close to the side wall of specimen #6-free ($x = 290$ mm). The side wall has the scan coordinate $x = 0$. The reconstruction area was extended

to the left side such that not only the area below the instrument but also a sideways area between $x = -200$ mm and $x = +290$ mm was included. In addition to the indications (1) from the backwall surface and (2) from the upper surfaces, there are signals (3), (4), and (5), which have the coordinates $x = 0$, and $z = 0$ mm, $z = 250$ mm, and $z = 500$ mm, respectively. All three indications are formed by the side wall as illustrated in the schematic sketch in Fig. 14b. Signal (3) is the reflection of the surface wave from the upper left corner of the block. Signal (4) is the corner echo, i.e., it is the reflection of the SH wave from the lower left corner. Signal (5) is the reflection of the bulk shear wave from the upper left corner of the block. In this case, the acoustic waves first reflect from the backwall surface before they reach the corner reflector and then again reflect from the backwall before they reach the receivers.

The extension of the reconstruction area in combination with a position of the instrument that is not above the corner but displaced by about $x = d$ allows a visualisation of the corner reflection. Figure 15a shows once more a SAFT-reconstruction of a single scan line taken on specimen #6-fdc with a full-depth crack. The reconstruction area was extended to the left and right sides. The indications of the corners of the specimen at $x = 0$ mm and $x = 1500$ mm are now clearly visible. The profile in Fig. 15b shows the amplitude maximum in the interval $z = 240$ – 270 mm (depth of the backwall indication). This profile also shows the corner echoes as well-defined peaks. It is clear however, that there is no change in

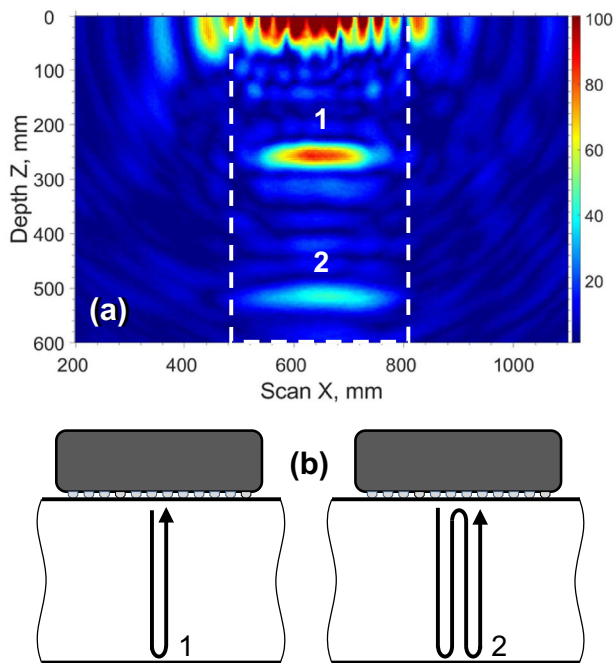


Fig. 13 **a** SAFT reconstruction without cosine filtering of one MIRA position on specimen #6-free before crack creation, instrument position $x = 650$ mm. The dashed lines show the area of 330 mm width below the instrument. **b** Schematic sound path of the indications in (a)

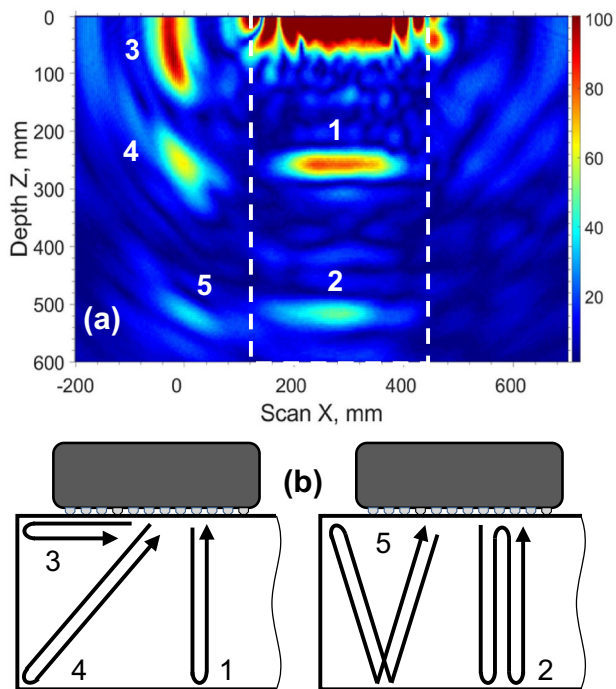


Fig. 14 **a** SAFT reconstruction without cosine filtering of one MIRA position on specimen #6-free before crack creation, instrument position $x = 290$ mm. The dashed lines show the area of 330 mm width below the instrument. **b** Schematic sound path of the indications in (a)

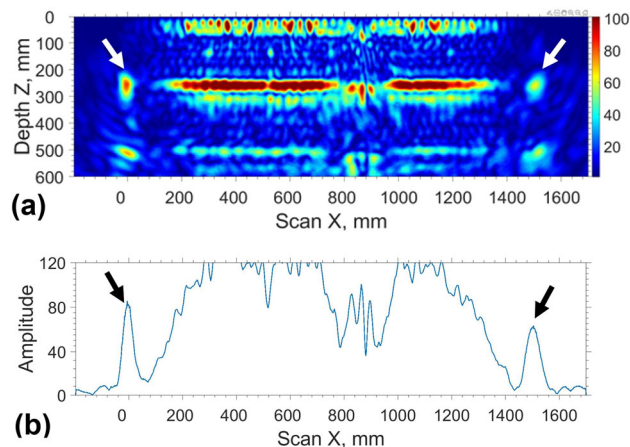


Fig. 15 **a** Compound-B-scan of specimen #6-fdc with a full-depth crack, reconstruction opening angle -90° to $+90^\circ$, and **b** amplitude profile at the depth interval 240 – 270 mm. White arrows in (a) and black arrows in (b): Corner indications from the side faces of the specimen (lower left and right corners)

the indication at the crack position at $x = 860$ mm (see Fig. 9 h). Reflections from the corners occur as indication at the same depth z as the echoes from the backwall. If an acoustic array is located above the corner or too close to it, the indication from the corner reflector merges with the backwall indication and cannot be detected.

A minimal distance or, from another point of view, a minimal angle between the corner reflector and the array shall be kept to ensure that these two indications can be distinguished. One solution would be to discard the positions above the crack position and use only a subset of the scan positions for the reconstruction. However, this solution is not optimal, since it is possible that the crack position is not exactly known. The problem can be solved if the backwall signal is removed from the image by limiting the reconstruction angles. As an example, Fig. 16 shows the compound-B-scan of one line scan of specimen #6-fdc with full-depth crack, and its amplitude profile at the depth interval around the back-wall indication. The angles of reconstruction were limited to $-60^\circ/-30^\circ$ and $30^\circ/60^\circ$. The angles are measured relative to the normal to the inspection surface.

As can be seen in Fig. 16, the backwall echo is filtered out and the corner reflections from the specimen edges and from the full-depth crack are still present. Some smaller indications from reinforcement bars close to the backwall are also visible. The profile in Fig. 16b shows the peaks of the specimen’s left edge ($x = 0$ mm) and right edge ($x = 1500$ mm) and of the full-depth crack at $x = 860$ mm. In the compound-B-scan, there are also indications at depth $z = 500$ mm from the upper specimen edges and from the upper crack corner.

Even more clearly, the crack profile can be imaged as a 2D SAFT C-scan. Figure 17 represents 2D SAFT C-scan projection images of an interval around the wall indication with

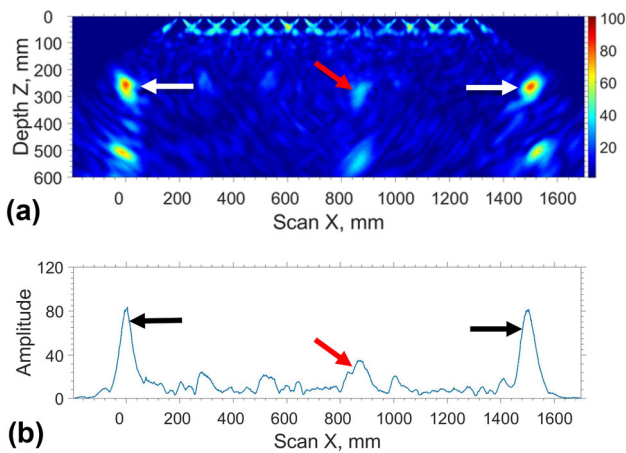


Fig. 16 **a** Compound-B-scan of specimen #6-fdc with full-depth crack, reconstruction opening angle $\pm (30^\circ\text{--}60^\circ)$, and **b** amplitude profile at the depth interval 240–270 mm. White arrows in **a** and black arrows in **b**: Corner indications from the side faces of the specimen (lower left and right corner), red arrows in **(a)** and **(b)**: Corner indication from the full-depth crack and the backwall

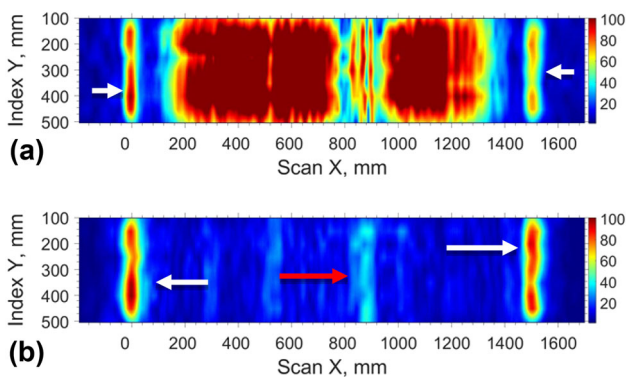


Fig. 17 Comparison of 2D SAFT C-scans (maximum of an interval of 240–270 mm depth) of specimen #6-fdc with a full-depth crack, with different reconstruction angles: **(a)** -90° to $+90^\circ$ and **(b)** $\pm(30^\circ\text{--}60^\circ)$. White arrows in **(a, b)**: Corner indications from the side faces of the specimen, red arrow in **(b)**: Corner indication from the full-depth crack

full angle of reconstruction (upper image) and with angular filtering (bottom image). The line at position $x = 860$ mm in the Fig. 17b is the reflection from the lower crack corner.

6 Application of SAFT with Angle Limitation

6.1 Examination of the 250 mm Thick Specimens with Respect to the Corner Indication

To compare the results on the objects with full-depth cracks and partial-depth cracks, we applied the backwall echo filtering and the corner echo extraction to the same ultrasonic data used for Fig. 9a–h. The results are displayed in Fig. 18.

From the images of Fig. 18, it can be stated that the corner reflections from the specimen's edges are presented in all compound-B-scans. The reflection intensity varies from specimen to specimen due the difference in the acoustical properties and the physical condition of the edges in this particular specimen slice ($y = 300$ mm). The second observation is that the compound-B-scans of the specimens with partial-depth cracks or notch have no indications between the edge indications at the depth which is equal to the specimen's thickness ($z = 250$ mm). On the other hand, in some compound scans there is a low-intensity indication at the depth $z = 500$ mm, which is the reflection from the upper crack/notch corner.

Figure 19 shows the 2D SAFT C-scan projections of the processed area scans with the angle limited to $\pm (30^\circ\text{--}60^\circ)$. A total of 9 lines with a distance of $\Delta y = 50$ mm were always acquired. The SAFT reconstructed data were evaluated in the depth interval between $z = 240$ mm and $z = 270$ mm. The edges of the samples are seen at the positions $x = 0$ mm and $x = 1500$ mm. As the roughness of the sidewalls and the scattering in the component vary, the intensity of the indication also varies for the different y -values (scan lines). The full-depth crack is visible as a line at $x = 860$ mm in Fig. 19h. The images of the other specimens are free of comparable indications at their corresponding defect position. The image of the reference specimen #4-free (Fig. 19d) is remarkable. The left corner indication of the specimen's edge is not complete, and there are strong indications between $x = 800$ mm and $x = 1200$ mm.

The detailed visual inspection of specimen #4-free provided explanation of the ultrasonic indications. One edge of the specimen was damaged, and a diagonal crack was visible at the side faces. Figure 20 shows photos of the two side faces with the damaged corner (black arrows) and the crack (red arrows). These defects explain the missing part of the corner indication at $x = 0$ in Fig. 19d.

For a further inspection, the specimen was rotated and positioned on its backwall. Cracks were found and documented, as seen in Fig. 21. These cracks were partial-depth cracks open to the backwall. This explains the findings in Fig. 9d, where the surface indications are free of disruption, while the backwall indication is interrupted. The corner echo indications in Fig. 19d match the crack opening in the backwall found by visual inspection as can be seen by comparing the green box in the schematic sketch of the visual inspection with the ultrasonic 2D SAFT C-scan in Fig. 21.

6.2 Application of SAFT with Angle Limitation to a Specimen with 500 mm Thickness

In order to examine the performance of the technique with thicker components, a 500 mm thick specimen with full-depth crack was fabricated by BAM. The specimen contains

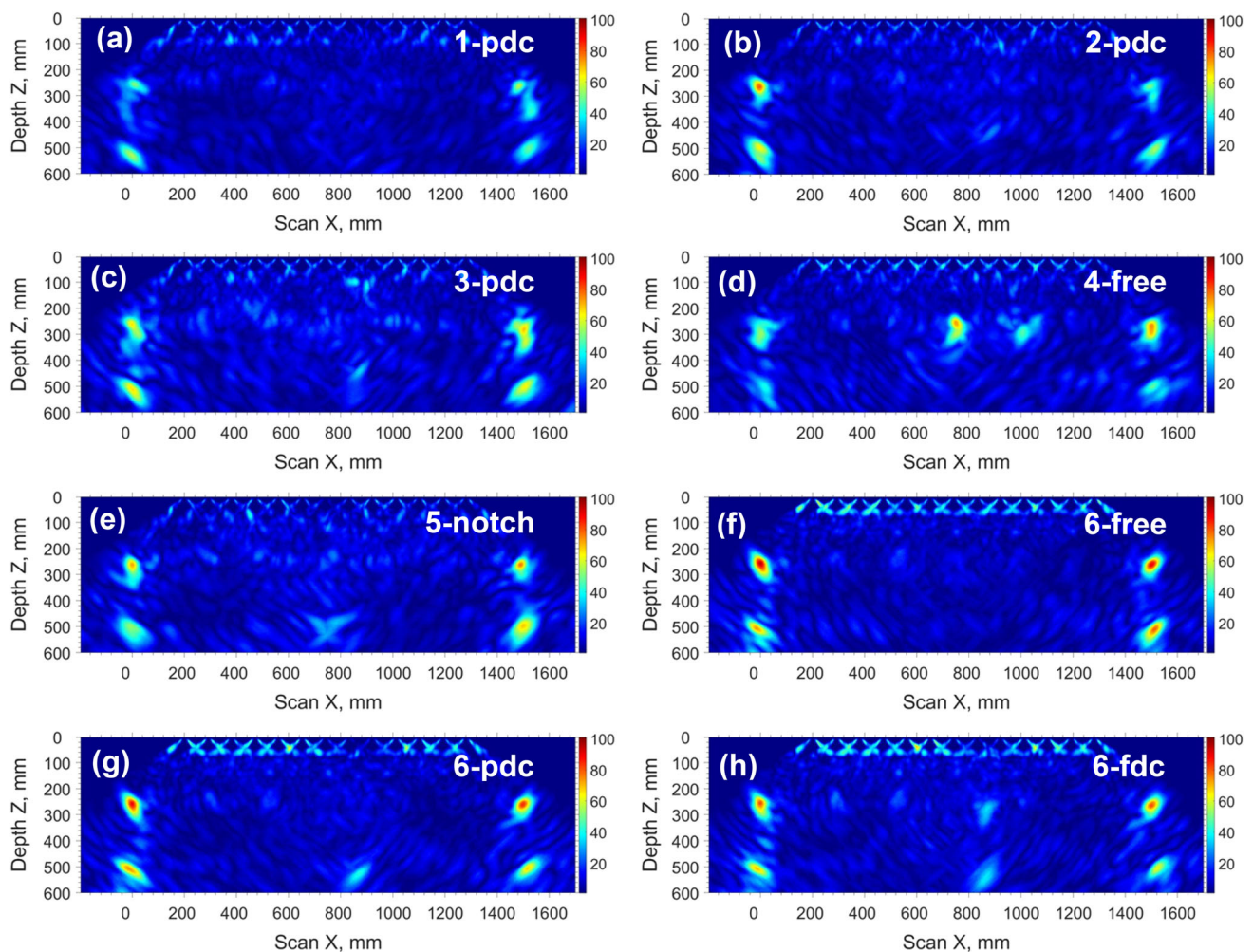


Fig. 18 Compound-B-scans images of the specimens listed in Table 1, one scan line ($y = 300$ mm), angle limitations $\pm (30^\circ - 60^\circ)$. **a–e** Specimen #1–#5. Specimen #6 was scanned and evaluated in three different

conditions: **f** without defect, **g** with partial-depth crack and **h** with full-depth crack

only two layers of reinforcement as shown in Fig. 22. The surface of the specimen was scanned with the MIRA before crack generation. With seven drill holes filled with expansion mortar, a full-depth crack was produced. Afterwards, more area scans were acquired.

After processing the MIRA data with the procedure explained above, the corner indications of the specimen's side faces are very well visible (Fig. 23). The indications are very strong and free of noise because the specimen contains less reinforcement bars than the 250 mm thick ones.

After the full-depth crack was produced, an additional indication appears approximately in the middle of the specimen at the crack's x -position (Fig. 24). The indications of the full-depth crack are also very strong and relatively free of noise. The amplitude of the crack indication varies depending on the y -position. Though the crack opening was mainly parallel to the y -direction because the drill holes specified

this direction, the crack front can deviate inside the specimen, and the walls do not need to be perfectly vertical and flat. Such roughness and deviation of the crack's side faces from the "ideal" orientation of a vertical wall can reduce the amplitude of the corner indication.

6.3 Application to 1000 mm Thick Round Foundation

The corner echo technique was tested further on a 1000 mm thick circular foundation located at the outdoor facility of the BAM. The foundation has a diameter of 4000 mm. Two rigid foam plates were embedded as models for vertical cracks. One of the plates (defect 2, representing a full-depth crack) had a height of 900 mm and a length of 800 mm, the other one had a height of 600 mm and a length of 800 mm (defect 1, model of partial-depth crack). The plates were fixed with their length axis in radial direction below the upper layer of

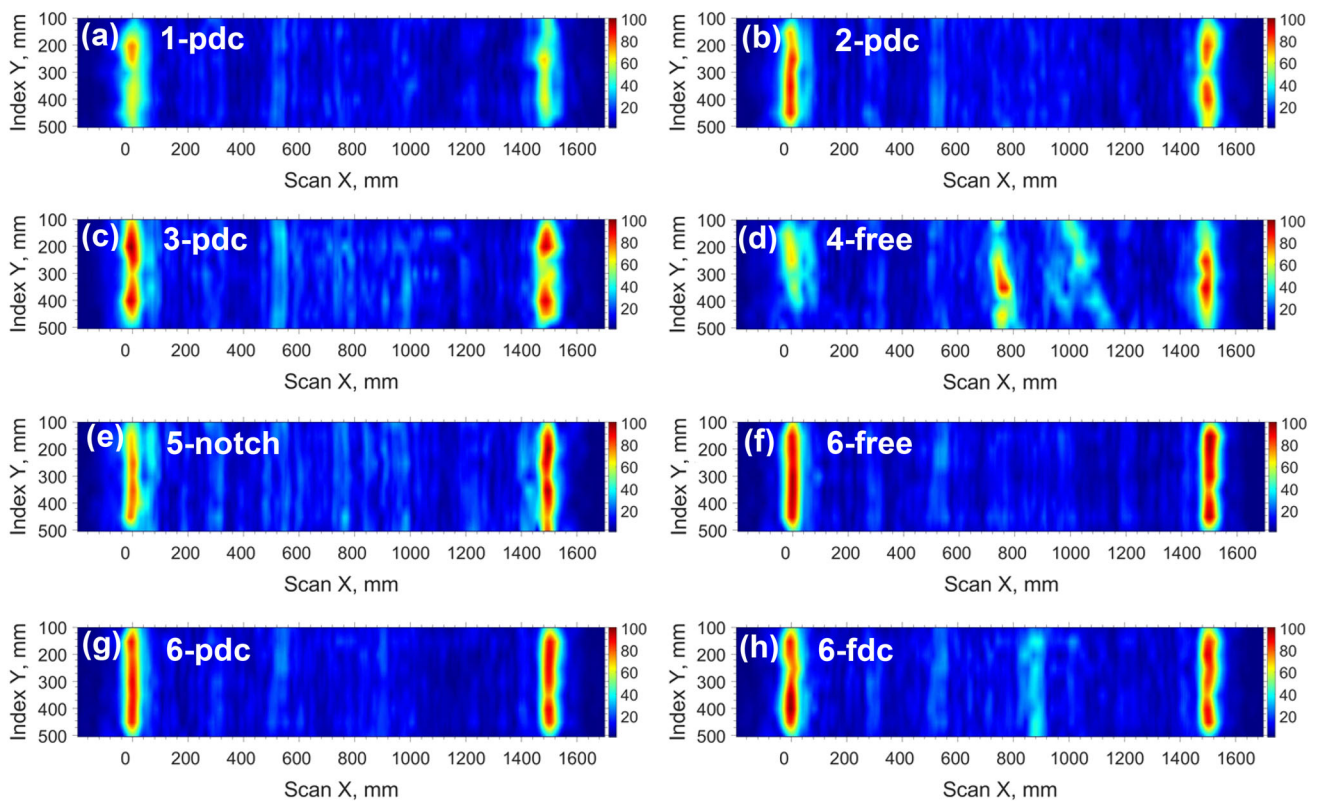


Fig. 19 2D SAFT C-scans of the specimens listed in Table 1, the angle of reconstruction was limited to $\pm (30^\circ\text{--}60^\circ)$. The evaluated depth interval is $z = 240\text{--}270$ mm. **a–e**: Specimen #1–#5. Specimen #6 is shown

in three different conditions: **f** without defect, **g** with partial-depth crack and **h** with full-depth crack

reinforcement (Fig. 25). After the concrete was cured, rectangular scan areas were defined on the top surface of the foundation above each of the test defects. Using the MIRA instrument, area scans were taken with a step size of 90 mm along the x -axis and 50 mm along the y -axis at a centre frequency of 50 kHz. Figures 26, 27 and 28 show the SAFT reconstruction results of the MIRA measurement data for defects 1 and 2. In this case, the software InterSAFT (K. Mayer, Kassel, Germany, [29]) available at BAM was used. This software also allows a selection of the angle of reconstruction. Other than the previous investigations, a 3D reconstruction was calculated. To visualise the corner echo of the vertical defects, an angle of ± 30 was defined in the SAFT software.

As can be seen in Figs. 26 and 27, both test defects deliver a corner indication. However, the magnitude of the indication of defect 2 is about 10 times higher than the magnitude of test defect 2. The respective SAFT-C-scans show that the indication of test defect 1 is not much higher than the noise level. A small indication in case of the 600 mm deep plate, which did not protrude to the backwall, can be explained by echoes from reinforcement bars and by ultrasonic rays which are reflected at the side wall of the corner formed by the

plate and the backwall (Δz -values larger than 165 mm, see Eq. 4 and Fig. 13). For geometrical reasons, the length of the scan lines perpendicular to the “crack opening” was limited, and the distance between the nominal position of the MIRA and the crack position was smaller than the recommended value of $d = 1000$ mm. In summary, the measurement on the 1000 mm thick foundation confirmed the applicability of the corner echo technique to thick-walled components.

7 Discussion and Outlook

In this work, we showed that the corner echo technique which is commonly used in ultrasonic testing of metals can be applied for ultrasonic testing of concrete with commercially available DPC shear wave arrays. The corner echo can be visualised using 2D or 3D SAFT processing of areas-scans, line-scans or single-point measurements with adapted parameters.

Either the position of the array relative to the corner can be selected, or the angle of reconstruction can be restricted to separate the corner indication from the backwall indication, or both methods can be combined. This procedure enables

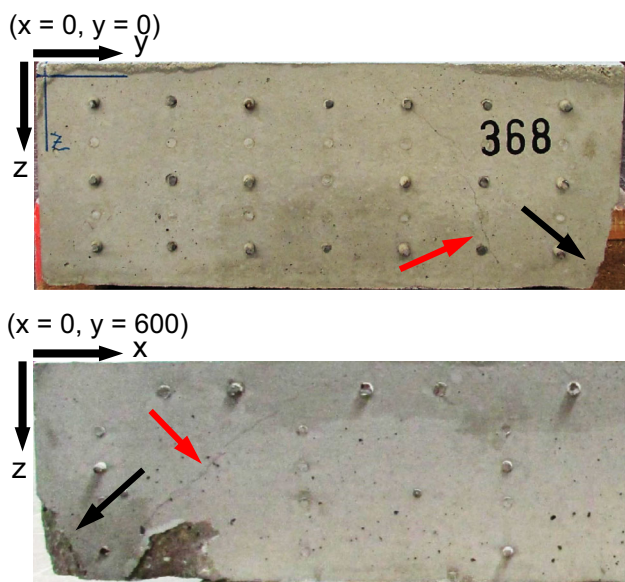


Fig. 20 Photos of the damaged edge of specimen #4-free with missing corner (black arrows) and crack (red arrows) (Color figure online)

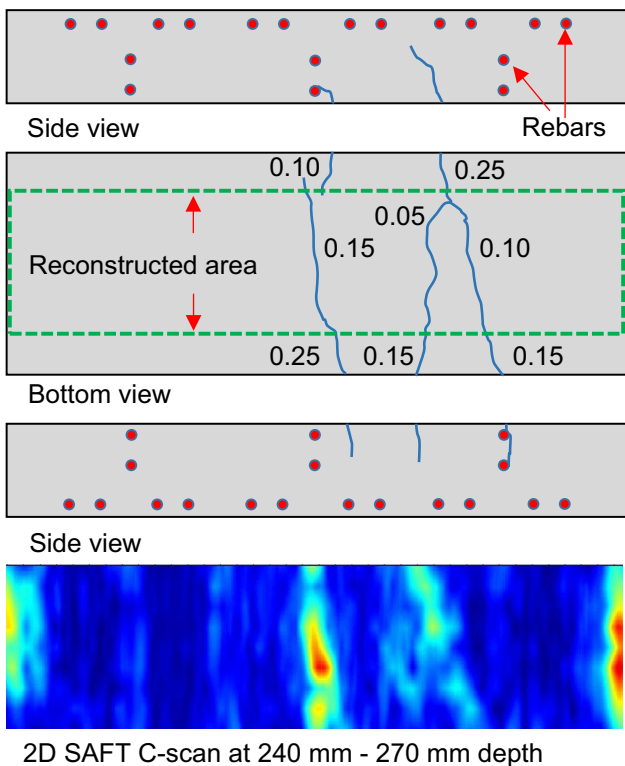


Fig. 21 Sketch of the results of the visual inspection of the backwall of specimen #4-free and ultrasonic SAFT-C-scan with angular filtering to display corner echoes. The black numbers are approximate crack opening values in mm

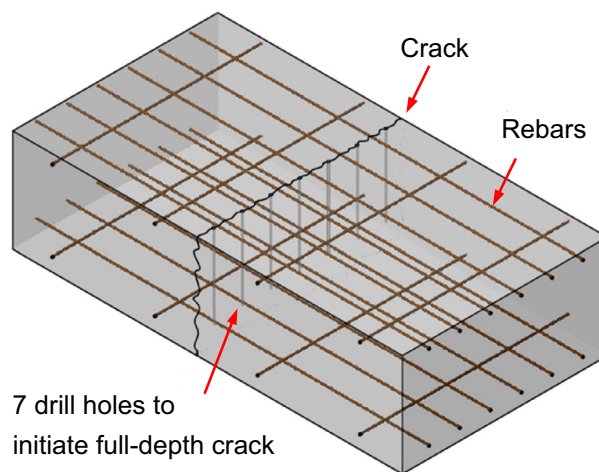


Fig. 22 Sketch of the 500 mm thick specimen #7 with full-depth crack

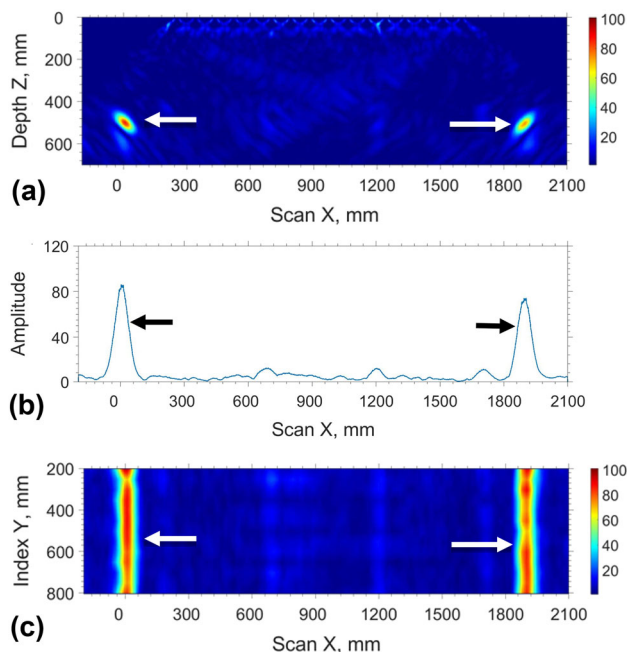


Fig. 23 Compound-B-scan, 2D SAFT C-scan with angular filtering and profile at depth $z = 470\text{--}540$ mm of the 500 mm thick specimen #7-free before crack generation. White and black arrows: Corner indications from the side faces of the specimen

application of the corner echo technique using commercially available measurement equipment and SAFT software. The results of this paper were demonstrated using the A1040 MIRA as an example, but they are applicable to other linear DPC arrays that use SH waves.

The side faces of block-shaped specimens are a good reference to probe corner echo detection. If the vertical walls are flat and exactly perpendicular to the backwall, the corner indication has the maximal intensity. For real cracks, the crack opening, the roughness or the crack’s sidewalls and

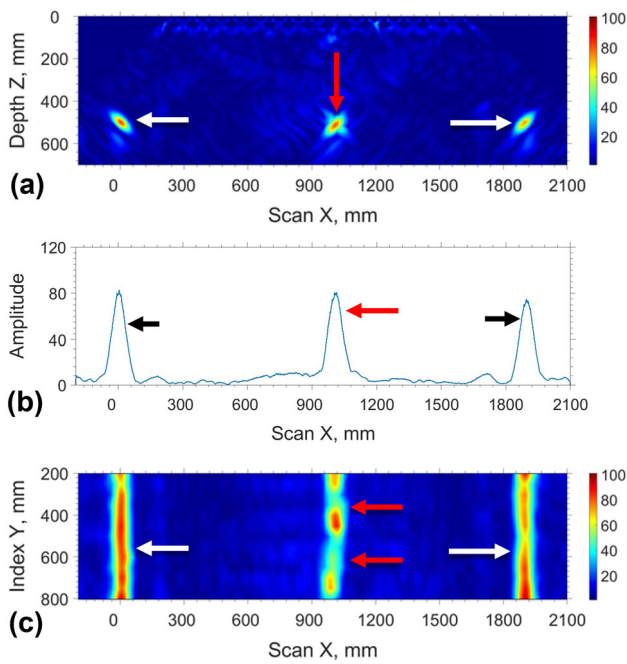


Fig. 24 Compound-B-scan, 2D SAFT C-scan with angular filtering and profile at depth $z = 470\text{--}540$ mm of specimen # 7-fdc with full-depth crack. White and black arrows: Corner indications from the side faces of the specimen, red arrows: Corner indications from the full-depth crack (Color figure online)

their orientation can vary from place to place. If the crack faces are rough such that they scatter the ultrasonic wave

instead of providing a specular reflection, or if the orientation of the crack faces deviates from the perpendicular orientation, the intensity of the corner indication reduces. Therefore, a single scan line perpendicular to the crack opening is often not enough, but rather, several scan lines or area scans are necessary to obtain more statistics.

For visualisation of the corner echo, the conventional SAFT reconstruction with limited angles was used, though the underlying hypothesis of direction independent secondary point sources (see Chapter 4) is not correct in case of a reflecting corner with a specular reflection at two points. Nevertheless, the corner indication was clearly visible, making a practical application possible. Within further work, an improvement of the corner indication is aimed using special algorithms. Additional examination is also needed to consider the effect of the inclination angle of the crack.

One application of the corner reflection method is a qualitative estimation of the depth of the crack. If the crack breaks both surfaces—the inspection surface and the backwall of the object—the conclusion can be made that the crack is a full-depth crack. For example, the crack opening can be visually identified on the inspection surface and on the backwall by using the corner reflection. Alternatively, the crack opening in the inspection surface can be confirmed through the corner reflection as well. For that, the reconstruction area is extended in z -direction such that the first mirror plane is included. The second corner reflection from the crack at the top surface (indication (5) in Figs. 14 and 16 as an example)

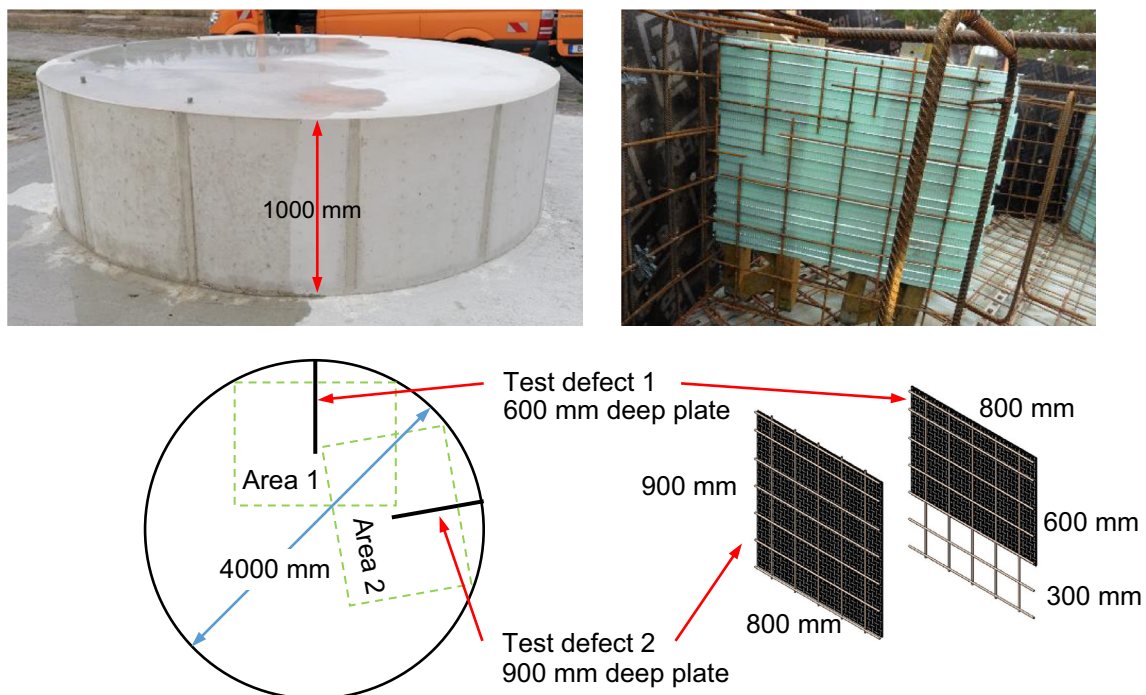


Fig. 25 Photo of the 1 m thick foundation located at the test facility BAM, Horstwalde, with two embedded foam plates as test defects. The plates were radially oriented and had different heights. Two areas were defined for MIRA measurements on the top surface of the foundation

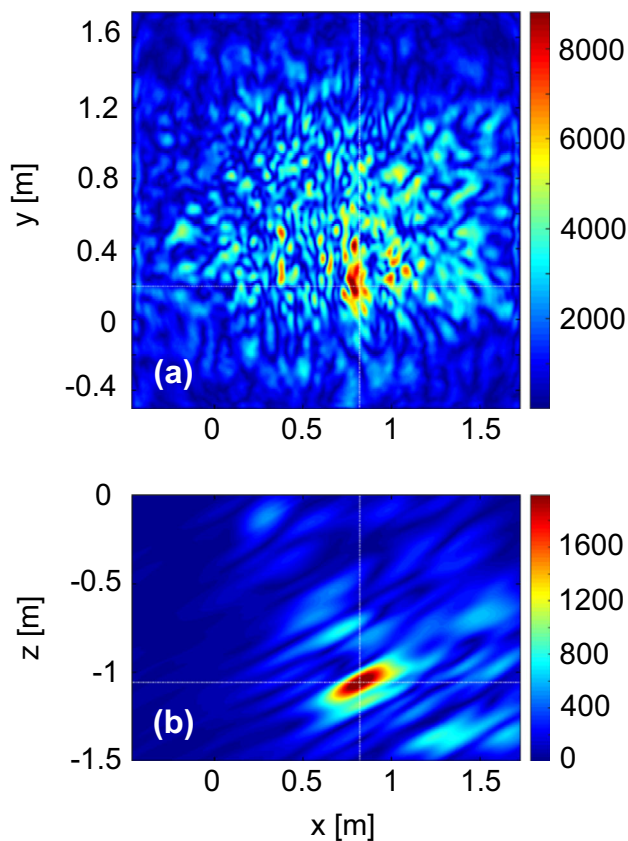


Fig. 26 3D SAFT reconstruction of the measurements in area 1 with angular filtering, **a** 3D SAFT C-scan at a depth of 1000 mm, **b** B-scan of corner echo

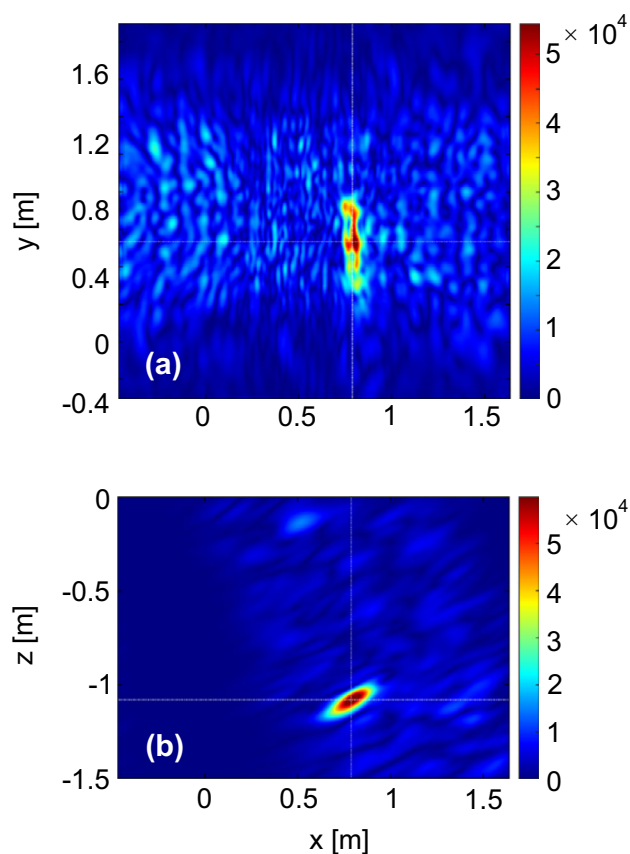


Fig. 27 3D SAFT reconstruction of the measurements in area 2 with angular filtering, **a** 3D SAFT C-scan at a depth of 1000 mm, **b** B-scan of corner echo

appears at the depth that corresponds the double thickness of the inspection object.

The presence of a corner echo reflection in the ultrasonic image is an indicator of a vertically oriented surface breaking flaw, like a crack. Thus, this technique can be used for detection of surface cracks in a concrete plate. If the exact location or even the presence of the crack is unknown, a single point measurement is not sufficient to detect the crack; it can be identified via a line-scan or an area-scan with additional limitation of the reconstruction opening angle. An important factor in case of unknown / invisible crack(s) is the requirement, that the ultrasonic device is oriented possibly orthogonal to the crack face to ensure that the sound reflects back to the array and not in any other direction. Therefore, scanning of the region of interest with various device orientation is recommended.

A few words should be added about the influence of rebars on the reliability of the inspection results. Rebars scatter the sound. That means, firstly, they reduce the acoustical energy, which arrives at the crack corner and—on the way back—at the receiver. Secondly, diffractions and reflections from rebars cause signals in A-scans and indications in the reconstructed SAFT images. The scattering of the acoustical

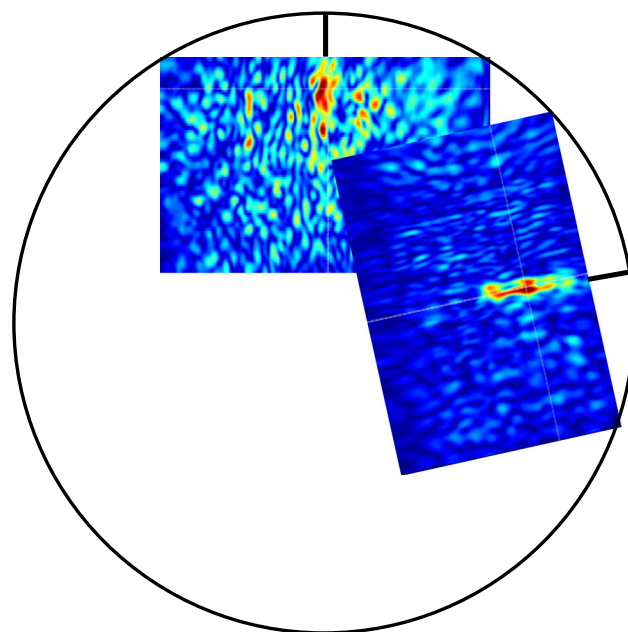


Fig. 28 SAFT-C-scans shown in the scan areas on top of the foundation

energy by rebars can be a limiting factor for any kind of concrete inspection, not only for the corner reflection method. An even more significant effect can be observed in the case of a very dense reinforcement layer. In the current study the reinforcement of the concrete blocks did not limit their testability.

The indications from rebars are visible in the reconstructed images. Nevertheless, they can be easily identified as rebars, since they are located at a depth which differs from the object thickness. Even if rebars are located close to the backwall, they can be separated from the crack indication due to their lower intensity in comparison to the corner reflection and thanks to their regular spatial arrangement (see Fig. 19 e.g.).

The MIRA instrument used here is applicable for components with maximal thickness of approximately 2000 mm. The exact penetration depth depends on the ultrasonic velocity of the component and on the scattering by rebars and grains. Though the linear array is predestined to steer into selected angles by post-processing of the data, application of other equipment like the Large Aperture Ultrasonic System (LAUS) [30, 31] should be considered for thick components.

In addition to the corner echo, other ultrasound methods like e.g., plane wave imaging [32] can be elaborated in the future to gain more information on crack depth. The crack tip echo was recently mapped for a real crack in concrete [33]. Other recent advanced developments such as targeted filtering and information fusion from different measurement methods [34], phase analysis of ultrasonic time signals [31], or extended synthetic aperture focusing technique [35], to name only a few, contribute to a general improvement of the signal-to-noise ratio in the nondestructive images of concrete and can be analysed with regard to their potential to improve crack depth measurements.

Acknowledgements We thank Sean Smith and Marco Lange, BAM, for manufacturing the specimens and application of the expansion mortar technique to produce the cracks. Lennart Friedrich, IZFP, was involved in the tedious acquisition of numerous line- and area scans. We especially thank Dr.-Ing. Klaus Mayer for detailed discussions regarding SAFT processing of ultrasonic data acquired on concrete.

Author Contributions Contributions of the authors: H.-G.H., EN: Supervision. P.P., S.P., U.R.: Investigation. S.P., U.R. and H.W.: Methodology and writing of original draft. All authors contributed to the text and reviewed the manuscript.

Funding Open Access funding enabled and organized by Projekt DEAL. No funding was provided for the preparation of this manuscript.

Data Availability A data set that supports the findings of this study is available from U.R. upon reasonable request.

Declarations

Competing interest One of the authors (E. N.) belongs to the editorial team of the journal.

Ethical Approval Not applicable.

Consent to Participate Not applicable.

Consent for Publication Not applicable.

Open Access This article is licensed under a Creative Commons Attribution 4.0 International License, which permits use, sharing, adaptation, distribution and reproduction in any medium or format, as long as you give appropriate credit to the original author(s) and the source, provide a link to the Creative Commons licence, and indicate if changes were made. The images or other third party material in this article are included in the article's Creative Commons licence, unless indicated otherwise in a credit line to the material. If material is not included in the article's Creative Commons licence and your intended use is not permitted by statutory regulation or exceeds the permitted use, you will need to obtain permission directly from the copyright holder. To view a copy of this licence, visit <http://creativecommons.org/licenses/by/4.0/>.

References

1. DIN EN 1992-1-1 Eurocode 2: design of concrete structures—Part 1–1: General rules and rules for buildings; German version (2010)
2. DBV B18, Risse in Beton, Zement-Merkblatt Betontechnik B 18 2.2020 (in German)
3. British Standard BS 1881, Testing Concrete, Part 203, 1986. Recommendations for measurement of velocity of ultrasonic pulses in concrete
4. Sansalone, M., Lin, J.-M., Streett, W.B.: Determining the depth of surface-opening cracks using impact-generated stress waves and time-of-flight techniques. *ACI Mater. J.* **95**, 168–177 (1998). <https://doi.org/10.14359/362>
5. Sun, Y., Huang, P., Su, J., Wang, T.: Depth estimation of surface-opening crack in concrete beams using impact-echo and non-contact video-based methods. *EURASIP J. Image Video Process.* (2018). <https://doi.org/10.1186/s13640-018-0382-7>
6. Popovics, J.S., Song, W.-J., Ghandehari, M., Subramaniam, K.V., Achenbach, J.D., Shah, S.P.: Application of surface wave transmission measurements for crack depth determination in concrete. *ACI Mater. J.* **97**, 127–135 (2000)
7. Ahn, E., Kim, H., Sim, S.-H., Shin, S.W., Popovics, J.S., Shin, M.: Surface-Wave based model for estimation of discontinuity depth in concrete. *Sensors* **18**, 2793 (2018). <https://doi.org/10.3390/s18092793>
8. Olson Instruments, Inc., Wheat Ridge, CO, USA, Impact Solenoids. <https://olsoninstruments.com/impact-devices/>, accessed March 24, 2023
9. Hévin, G., Abraham, O., Pedersen, H.A., Campillo, M.: Characterization of surface cracks with Rayleigh waves: A numerical model. *NDT & E Int.* **31**, 289–297 (1998). [https://doi.org/10.1016/S0963-8695\(98\)80013-3](https://doi.org/10.1016/S0963-8695(98)80013-3)
10. Kee, S.-H., Zhu, J.: Using air-coupled sensors to determine the depth of a surface-breaking crack in concrete. *J. Acoust. Soc. Am* **127**, 1279–1287 (2010). <https://doi.org/10.1121/1.3298431>
11. In, C.-W., Schempp, F., Kim, J.-Y., Jacobs, L.J.: A fully non-contact, air-coupled ultrasonic measurement of surface breaking cracks in concrete. *J. Nondestruct. Eval* **34**, 272 (2015). <https://doi.org/10.1007/s10921-014-0272-6>
12. Ramamoorthy, S.K., Kane, Y., Turner, J.A.: Ultrasonic diffusion for crack depth determination in concrete. *J. Acoust. Soc. Am* **115**, 523–529 (2004). <https://doi.org/10.1121/1.1642625>

13. Chi-Won In, Kevin Arne, Jin-Yeon Kim, Kimberly E. Kurtis, Laurence J. Jacobs, Estimation of Crack Depth in Concrete Using Diffuse Ultrasound: Validation in Cracked Concrete Beams, *J. Nondestruct. Eval.* **36** (2017) 4, <https://doi.org/10.1007/s10921-016-0382-4>
14. Quiviger, A., Payan, C., Chaix, J.-F., Garnier, V., Salin, J.: Effect of the presence and size of a real macro-crack on diffuse ultrasound in concrete. *NDT & E Int.* **45**, 128–132 (2012). <https://doi.org/10.1016/j.ndteint.2011.09.010>
15. Kozlov, V.N., Samokrutov, A.A., Shevaldykin, V.G.: Thickness measurements and flaw detection in concrete using ultrasonic echo method. *Nondestruct. Test. Eval.* **13**, 73–84 (1997). <https://doi.org/10.1080/02780899708953020>
16. De La Haza, A.O., Samokrutov, A.A., Samokrutov, P.A.: Assessment of concrete structures using the MIRA and Eyecon ultrasonic shear wave devices and the SAFT-C image reconstruction technique. *Construct. Build. Mater.* **38**, 1276–1291 (2013). <https://doi.org/10.1016/j.conbuildmat.2011.06.002>
17. Choi, P., Kim, D.-H., Lee, B.-H., Wong, M.C.: Application of ultrasonic shear-wave tomography to identify horizontal crack or delamination in concrete pavement and bridge. *Construct. Build. Mater.* **121**, 81–91 (2016). <https://doi.org/10.1016/j.conbuildmat.2016.05.126>
18. Felice, M.V., Velichko, A., Wilcox, P.D.: Accurate depth measurement of small surface-breaking cracks using an ultrasonic array post-processing technique. *NDT & E Int.* **68**, 105–112 (2014). <https://doi.org/10.1016/j.ndteint.2014.08.004>
19. Krause, M., Mielentz, F., Milmann, B., Müller, W., Schmitz, V.: Imaging of cracks and honeycombing in concrete elements, in: *Acoustical Imaging*, Arnold, W., Hirsekorn, S. (eds.), 129–137 (2004). https://doi.org/10.1007/978-1-4020-2402-3_17
20. Friese, M., Vogdt, F.U., Wiggemhauser, H.: Qualitätssicherung für Rissfüllungen: Ein neuer Ansatz mit bildgebende Ultraschallverfahren. *Beton- und Stahlbetonbau* **106**, 471–480 (2011). <https://doi.org/10.1002/best.201100029>
21. Wiggemhauser, H., Köpp, C., Timofeev, J., Azari, H.: Controlled creating of cracks for non-destructive testing. *J. Nondestruct. Eval.* (2018). <https://doi.org/10.1007/s10921-018-0517-x>
22. Miller, G.F., Pursey, H.: The field and radiation Impedance of mechanical radiators on the free surface of a semi-infinite isotropic solid. *Proc. R. Soc. Lond. A* **223**, 521–541 (1954). <https://doi.org/10.1098/rspa.1954.0134>
23. Shevaldykin, V.G., Samokrutov, A.A., Kozlov, V.N.: Ultrasonic low-frequency transducers with dry dot contact and their application for evaluation of concrete structures. *Proc. IEEE Ultrasonics Symp.* (2002). <https://doi.org/10.1109/ULTSYM.2002.1193518>
24. Mielentz, F., Feller, V., Krause, M., Orglmeister, R., Mayer, K.: Schallfeldmodellierung von Ultraschall-Transversalwellen-Prüfköpfen. *Mater. Test.* **55**, 856–864 (2013). <https://doi.org/10.3139/120.110510>
25. Corl, P.O., Grant, P.M., Kino, G.S.: A Digital synthetic focus acoustic imaging system for NDE. *IEEE Ultrasonics Symp.* (1978). <https://doi.org/10.1109/ULTSYM.1978.197042>
26. Holmes, C., Drinkwater, B.W., Wilcox, P.D.: Post-processing of the full matrix of ultrasonic transmit-receive array data for non-destructive evaluation. *NDT & E Int.* **38**, 701–711 (2005). <https://doi.org/10.1016/j.ndteint.2005.04.002>
27. The MathWorks, Inc. (2023). MATLAB version: 9.9.0 (R2020b) <https://www.mathworks.com>, accessed March 21, 2023
28. Krautkrämer, J., Krautkrämer, H.: *Ultrasonic Testing of Materials*. Springer, Berlin (1990)
29. Krause, M., Mayer, K., Chinta, P.K., Effner, U.: Ultrasonic imaging of defects in building elements made from timber. *Adv. Mater. Res.* **778**, 312–320 (2013). <https://doi.org/10.4028/www.scientific.net/AMR.778.312>
30. Wiggemhauser, H., Samokrutov, A., Mayer, K., Krause, M., Alekhin, S., Elkin, V.: Large aperture ultrasonic system for testing thick concrete structures. *J. Infrastr. Syst.* (2017). [https://doi.org/10.1061/\(ASCE\)IS.1943-555X.0000031](https://doi.org/10.1061/(ASCE)IS.1943-555X.0000031)
31. Lay, V., Effner, U., Niederleithinger, E., Arendt, J., Hofmann, M., Kudla, W.: Ultrasonic quality assurance at magnesia shotcrete sealing structures. *Sensors* **11**, 8717 (2022). <https://doi.org/10.3390/s22228717>
32. S.T. Kuchipudi, D. Ghosh, An ultrasonic wave-based framework for imaging internal cracks in concrete, *Struct. Control Health Monit.* 2022, e3108, <https://doi.org/10.1002/stc.3108>
33. Bulavinov, A., Pinchuck, R., Samokrutov, A., Shevaldykin, V.: Advanced tomographic imaging techniques for quality assessment of concrete structures by means of ultrasound. In: *Proceedings of the International Conference on Non-destructive Evaluation of Concrete in Nuclear Applications*, January 25–27, 2023, Espoo, Finland, *NDE NucCon 2023*, pp. 213–220. <https://www.aalto.fi/en/nde-nucon-2023>, accessed March 24, 2023
34. Mehdinia, S., Schumacher, T., Song, X., Wan, E.: A pipeline for enhanced multimodal 2D imaging of concrete structures. *Mater. Struct.* **54**, 228 (2021). <https://doi.org/10.1617/s11527-021-01803-w>
35. Hoegh, K., Khazanovich, L.: Extended synthetic aperture focusing technique for ultrasonic imaging of concrete. *NDT & E Int.* **74**, 33–42 (2015). <https://doi.org/10.1016/j.ndteint.2015.05.001>

Publisher's Note Springer Nature remains neutral with regard to jurisdictional claims in published maps and institutional affiliations.